



**Tuning Coordination Modes of Pyridine/Thioether Schiff
Base (NNS) Ligands to Mononuclear Manganese Carbonyls**

Journal:	<i>Dalton Transactions</i>
Manuscript ID:	DT-ART-02-2014-000600.R1
Article Type:	Paper
Date Submitted by the Author:	18-Apr-2014
Complete List of Authors:	Lumsden, Simone; The University of Texas at Austin, Department of Chemistry Durgaprasad, Gummadi; The University of Texas at Austin, Department of Chemistry Thomas Muthiah, Keren; The University of Texas at Austin, Department of Chemistry Rose, Michael; The University of Texas at Austin, Department of Chemistry

Tuning Coordination Modes of Pyridine/Thioether Schiff Base (NNS) Ligands to Mononuclear Manganese Carbonyls

Simone E. A. Lumsden, Gummadi Durgaprasad, Keren A. Thomas Muthiah
and Michael J. Rose*

Department of Chemistry, The University of Texas at Austin

*corresponding author: mrose@cm.utexas.edu

Abstract

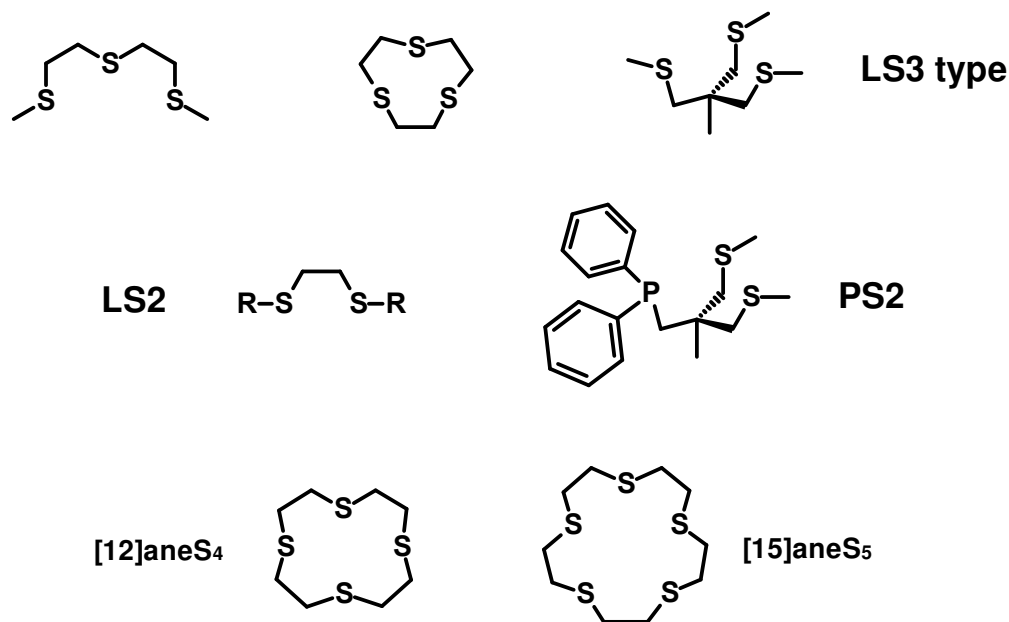
We have investigated the coordination modes of NNS Schiff base, thioether ligands to manganese(I) carbonyls. The ligands contain *ortho* substituted pyridines (H, CH₃, OCH₃, fluorophenyl) and varying substituents (H, CH₃) at the Schiff base linkage. In general, reaction of [Mn(CO)₅Br] with a tridentate NNS ligand in CH₂Cl₂ affords species in which the thioether-S may be bound or unbound at the manganese center, depending on the steric and electronic substitution in the ligand framework; as a result, the complexes exhibit two or three carbonyl ligands, respectively. Aldehyde-derived ligand frames (R₁N_HNS) generally afford complexes of type [(R₁NNS)Mn(CO)₃Br] (**1**_{CO}, **2**_{CO}, **3**_{CO}; R = H, OCH₃, CH₃) that exhibit incomplete ligation of the chelate (S not bound) in X-ray structures. In contrast, use of the iminomethyl ligand (N_{Me}NS) affords a complex of formula [(N_{Me}NS)Mn(CO)₂Br] (**4**_{CO}), in which the mixed N/thioether-S stabilizes the {Mn(CO)₂}⁺ fragment. In solid state IR spectra, complexes of type [(R₁NNS)Mn(CO)₃Br] (**1**_{CO} through **3**_{CO}) afford three ν(CO) in the range ~2060-1865 cm⁻¹; the dicarbonyl complex [(N_{Me}NS)Mn(CO)₂Br] (**4**_{CO}) exhibits two carbonyl stretches in the range ~1920-1845 cm⁻¹. Prolonged storage of the tricarbonyl [(MeNNS)Mn(CO)₃Br] (**3**_{CO}) in presence of trace dioxygen affords the dibromide species [(MeNNS)Mn(Br)₂] (**3**_{Br}), in which the thioether S reliably binds to the Mn(II) center. Complexes **1**_{CO}-**3**_{CO} exhibit simple, diamagnetic ¹H NMR spectra in CD₂Cl₂. The S-ligated complex **4**_{CO} exhibits spectra consistent with a mixture of an S-bound (6-coordinate) and S-unbound (5-coordinate) species as represented by [(N_{Me}NS)Mn(CO)₂Br] ↔ [(N_{Me}NS)Mn(CO)₂Br]. Lastly, we obtained crystal structures of the S-bound and S-unbound conformers derived from *the same* ligand – the fluorophenyl derived FPhNNS, namely [(FPhNNS)Mn(CO)₃Br] (**5**_{CO-a}) and [(FPhNNS)Mn(CO)₂Br] (**5**_{CO-b}). This report represents several examples of a thioether-stabilized {Mn(CO)₂}⁺ fragment, a deviation from the usual 'piano stool' Mn(I) tricarbonyl motif. Overall, we highlight that coordination of these NNS ligands to Mn(I) carbonyls occurs on a soft conformational landscape, and that ligand substituents can be rationally employed to favor the desired coordination mode.

Introduction

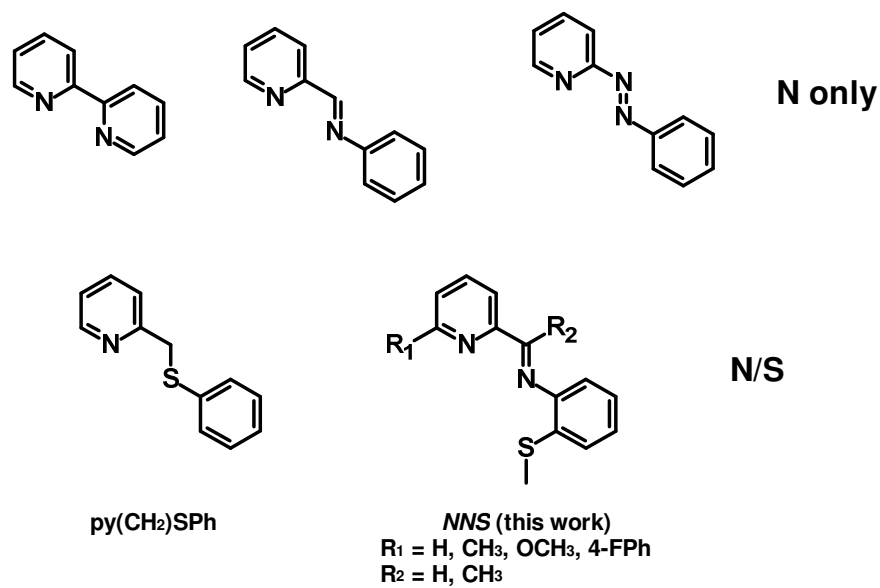
The coordination chemistry of manganese(I) carbonyls has been explored because of their utility as catalysts (both homogeneous¹ and heterogeneous²), in the detection and delivery of carbon monoxide,³ as well as studies in fundamental coordination chemistry. Coordination complexes of manganese carbonyls have found use in carbon-carbon bond forming reactions,⁴ as well as the study of redox-active ligands.⁵ Organometallic species of manganese carbonyls have also been explored in catalytic hydrosilylations⁶ and alcoholysis of silanes.⁷ More recently, manganese carbonyls derived from bpy (2,2'-bipyridine) have been used in place of rhenium carbonyls in the electrocatalytic reduction of CO₂ to CO,⁸ a promising direction for energy-related catalysis by earth abundant metals.⁹

In our research, we are interested in the fundamental coordination chemistry of multi-dentate ligands bearing nitrogen and sulfur donors to mononuclear metal carbonyls of the late first row. The low-spin, d^6 configuration of Mn(I) carbonyls makes them amenable to isolation and solution studies. The carbonyls of Mn(I) are isoelectronic with their Fe(II) counterparts, and therefore exhibit some similar structural and donor preferences. However mononuclear Fe(II) carbonyls derived from coordinating ligands with nitrogen and sulfur donors – and that are free from stabilizing phosphines – are less represented in literature. Such iron complexes (especially mononuclear species) can be challenging to isolate, requiring low temperatures and dark conditions.¹⁰⁻¹⁵ In contrast, the Mn(I) carbonyls are thermally stable under ambient conditions in non-coordinating solvents, and exhibit a reduced sensitivity to light. Therefore, as an entry point to iron chemistry, we wished to explore the coordination of a tridentate NNS ligand frame with manganese carbonyls.

Inspection of crystallographically characterized thioether Mn(I) carbonyls reveals several interesting trends. Cationic complexes of Mn(I) carbonyls with fully bound thioether-S ligation have been previously reported,¹⁶⁻¹⁷ as in the case of $[(LS3)Mn(CO)_3]^+$, where the identities of LS3 are given below. Select examples of complete LS2 ligation to neutral complexes also exist, as in the case of $[(LS2)Mn(CO)_3X]$ ($R = CH_3, Ph; X = Cl, Br, respectively$).¹⁸ However, incomplete ligation of thioether chelates is very common, especially in neutral complexes. For example, the supporting tripodal ligand in $[(PS2)Mn(CO)_3Br]$ and the tetrapodal $[(LS4)Mn(CO)_3Cl]$ and leave one or two (respectively) thioether-S donor(s) unbound.^{19,20} This occurs even in some cationic complexes: the crown-type complexes $[[12]aneS_4)Mn(CO)_3]^+$ and $[[15]aneS_{3/5})Mn(CO)_3]^+$ also exhibit one and two unbound thioether(s) (respectively).²¹ Treatment of $[[12]aneS_{3/4})Mn(CO)_3]^+$ with Me_3NO did provide the dicarbonyl species $[[12]aneS_{4/4})Mn(CO)_2]^+$, wherein all 4 thioether-S were bound.²¹ Indeed, the authors of this report noted this was the first report of a thioether-stabilized $\{Mn(CO)_2\}^+$ fragment, which is typically only stabilized by phosphines and other strong σ -donating, π -accepting ligands. The $\{Mn(CO)_2\}^+$ fragment formed spontaneously under metalation conditions, although photolysis or exchange of coordinating solvent (MeCN, THF) can readily afford the $\{Mn(CO)_2\}^+$ unit in some cases.²²



During the course of this work, Mascharak and co-workers reported the preparation of several manganese(I) carbonyls derived from Schiff base ligands, and their utility as photo-releasing CO reagent molecules (photoCORMs).²³ Related photoactive manganese(I) tricarbonyls were also derived from diazopyridine, diimine N₂, and N₃ ligands.²³⁻²⁵ Most relevant to this work are complexes derived from similar Schiff base ligands with a pendant thioether-S. In the two cases of $[(L_{\text{NNS}})\text{Mn}(\text{CO})_3]^+$ ($L = \text{pmtpm}$ and qmtpm ; NNS and QNNS in our nomenclature), the thioether remained unbound.²³ Indeed, to date there is just a single example of a mixed N/S(thioether) ligand fully bound in a mononuclear complex, namely the complex $[(\text{py}(\text{CH}_2)\text{SPh})\text{Mn}(\text{CO})_3\text{Br}]$.²⁶ Also, irrespective of ligand choice (N₂S, N₂, or N₃) in all of these cases, only the tricarbonyl 'piano stool' congeners were isolated.



In this work, we attempted to circumvent difficulties associated with iron carbonyl chemistry, and utilize the more reliably mononuclear manganese congeners to explore the fundamental coordination chemistry of **NNS** type Schiff base ligands with metal carbonyls. As dimers readily form across thiolato-S bridges, we have also chosen a thioether moiety to allow for a sulfur donor, but to retain mononuclear motifs. As discussed above, the thioether-S displays a low binding affinity for Mn(I), often remaining unbound even when present in a tight-binding chelate (e.g. when an ideal 5-member chelate ring possible). Our work is focused on ligand optimization (steric and electronic tuning) to ensure complete ligation of the chelate to the metal center, as well as structural and spectroscopic characterization of the resulting complexes. Herein, we show that careful selection of the ligand substituents (see substituted **NNS** framework above) leads to not only the fully bound **NNS** coordination motif, but also to a new example of a thioether-stabilized $\{\text{Mn}(\text{CO})_2\}^+$ motif in the obligatory *cis* arrangement.

Experimental

General Procedures. The manganese starting material $[\text{Mn}(\text{CO})_5\text{Br}]$ was obtained from Strem Chemicals. All other reagents were obtained from Sigma Aldrich or Acros and used without further purification. For ligand preparation, solvents (MeOH, CH_2Cl_2 , AcOH) were purchased from Fisher and used without further purification. For metalation reactions, the CH_2Cl_2 , Et_2O and pentane were dried over an alumina column under argon atmosphere. All metalations and crystallizations were performed under N_2 atmosphere. Deuterated solvents were obtained from Cambridge Isotopes or Acros Organics. Several aldehyde-derived ligands (NNS and MeNNS) were prepared according to literature reports.^{27,28} We independently devised an analogous synthesis of $[(\text{NNS})\text{Mn}(\text{CO})_3\text{Br}]$ compared with a recently published report.²³

Ligands

OMeNNS . 1-(6-methoxy-2-pyridyl)-*N*-(2-methylsulfanylphenyl)methanimine. A batch of 6-methoxy-2-pyridinecarboxaldehyde (2.00 g, 14.6 mmol) was dissolved in 20 mL of MeOH. To this stirred solution was added a solution of 2-(methylthio)aniline (2.03 g, 14.6 mmol) in 15 mL of MeOH. The solution was heated to reflux temperature for 2 h, at which point the solution was cooled to ambient temperature and solvent evaporated under a stream of N_2 gas. The resulting tacky solid was gently triturated 2× with Et_2O to yield an orange solid. Selected IR bands (ν in cm^{-1}): 1623 w, 1587 m, 1567 s, 1462 s, 1439 s, 1321 m, 1138 w, 800 vs, 750 vs, 725 vs, 635 w, 538 m. ^1H NMR in CDCl_3 (δ from TMS): 8.44 s (1H), 7.90 d (1H), 7.68 t (1H), 7.23 br (1H), 7.16 br (1H), 7.08 br (1H), 6.82 d (1H), 6.75 br (1H), 4.00 s (3H), 2.47 s br (3H). HRMS calcd: 257.0749, 258.0827, 259.0905; found: 257.0756, 258.0833, 259.0903. NMR analysis indicated

unreacted (~30%) aldehyde that was not separated by fractional crystallization or chromatography. The mixture was used in subsequent metalations.

FPhNNS. *N-((6-(4-Fluorophenyl)pyridin-2-yl)methylene)-2-(methylthio)aniline.* A small batch of 6-(4-fluorophenyl)-2-pyridinecarboxaldehyde (0.289 g, 1.434 mmol) was dissolved in 25 mL of MeOH. To this stirred solution was added a solution of 2-(methylthio)aniline dissolved in 5 mL of MeOH. The reaction mixture was gently refluxed for 1 h, and then the solvent removed in vacuo. The resulting residue was washed with a small portion of cold pentane, and the product was collected as a yellow solid. Yield: 351 mg (76%). Selected IR bands (ν in cm^{-1}): 1622 m, 1600 m, 1586 m, 1451 s, 1351 w, 1213 s, 810 vs, 642 w, 566 s. ^1H NMR in CDCl_3 (δ in ppm from TMS): 8.64 s (1H), 8.25 d (1H), 8.03 dd (2H), 7.90-7.84 m (2H), 7.73 d (1H), 7.32 s br (1H), 7.16 t (1H), 7.10 m br (2H) 6.70 s br (1H), 2.46 s (3H). HRMS calcd: 321.0862, 322.0940, 323.1018; found: 321.0860, 322.0939, 323.1010.

N_{Me}NS. *2-(methylthio)-N-(1-(pyridin-2-yl)ethylidene)aniline.* The 2-(methylthio)aniline (0.500 g, 3.59 mmol) was diluted in 5 mL of acetic acid, and to this solution was added 2-acetylpyridine (0.434 g, 3.59 mmol) in 5 mL of AcOH. Next, a slurry of ZnCl_2 (0.489 g, 3.59 mmol) in 5 mL of AcOH was added, and the reaction refluxed for 1 h to generate an orange solution (when hot). Upon cooling a yellow solid forms, which was collected by filtration and washed with several portions of Et_2O . The solid was then dissolved in CH_2Cl_2 (25 mL) and washed 2 \times in a separatory funnel with 0.25 M $\text{K}_2\text{C}_2\text{O}_4$, and 2 \times with water. The organic layer was dried over Na_2SO_4 and evaporated to dryness by rotary evaporation to afford a yellow oil. Yield: 0.49 g (56%). Selected IR bands (ν in cm^{-1}): 3052 w, 2919 w, 1635 s, 1578 m, 1565 m, 1466 s,

1434 s, 1301 m, 993 w, 965 w, 780 vs, 737 vs, 649 w, 621 m. ^1H NMR in CDCl_3 (δ in ppm from TMS): 8.66 d (1H), 8.39 d (1H), 7.79 t (1H), 7.36 dt (1H), 7.25 d (1H), 7.14 m (2H), 6.72 d (1H), 2.37 s (3H), 2.34 (3H). HRMS calcd: 241.0799, 242.0878, 243.0956; found: 241.0802, 242.0878, 243.0959.

Complexes

[(NNS)Mn(CO)₃Br] (1_{CO}). Under N_2 atmosphere, 0.130 g (0.471 mmol) of $[\text{Mn}(\text{CO})_5\text{Br}]$ is stirred in 10 mL of DCM in a round bottom flask until a clear yellow-orange solution is obtained. In a separate round bottom flask, 0.110 g (0.482 mmol) of ligand is dissolved in another 10 mL of CH_2Cl_2 to generate a yellow solution. The ligand/ CH_2Cl_2 solution is added dropwise to the $[\text{Mn}(\text{CO})_5\text{Br}]$ solution. The mixture stirred overnight and there was a slow color change from yellow to a dark red solution. The dark solution was subjected to vapor diffusion of pentane at room temperature, which resulted in small black/red crystals suitable for X-ray diffraction. Yield: 71 mg (34%). Selected IR bands (ν in cm^{-1} , ν_{CO} in italics): 2023 *m*, 1918 *s*, 1867 *s*, 1590 *w* (ν_{CN}), 1415 *w*, 962 *w*, 767 *s*, 581 *m*. UV/vis in CH_2Cl_2 , λ in nm (ϵ in $\text{cm}^{-1} \text{M}^{-1}$): 323 (19 900); also see Table 3. ^1H NMR in CD_2Cl_2 (δ from TMS): 9.27 *s* (1H), 8.99 *s* (1H), 8.48 *s* (1H), 8.08 *m* (2H), 7.78-7.32 *m* (3H), 2.54 *s* (3H). Elemental Analysis, calcd: C 42.97, H 2.70, N 6.26; found: C 42.82, H 2.71, N 6.50.

[(MeONNS)Mn(CO)₃Br] (2_{CO}). Under N_2 atmosphere, 0.078 g (0.284 mmol) of $[\text{Mn}(\text{CO})_5\text{Br}]$ is stirred in 10 mL of DCM in a round bottom flask until a clear yellow-orange solution is obtained. In a separate round bottom flask, 0.071 g (0.275 mmol) of MeONNS ligand is dissolved in another 10 mL DCM to generate a pale yellow solution. The ligand/DCM solution is added dropwise to

the $[\text{Mn}(\text{CO})_5\text{Br}]$ solution. The mixture stirred overnight and there was a slow color change from yellow to a dark blood-red solution. The dark solution was subjected to vapor diffusion of pentane at room temperature, which resulted in small red cubic crystals suitable for X-ray diffraction. Yield: 70 mg (54%). Selected IR bands (ν in cm^{-1} , ν_{CO} in italics): 2056 *s*, 1934 *s*, 1905 *vs*, 1619 *w* (ν_{CN}), 1478 *s*, 1306 *m*, 957 *w*, 627 *s*, 455 *w*. UV/vis in CH_2Cl_2 , λ in nm (ϵ in $\text{cm}^{-1} \text{M}^{-1}$): 354 (4 070); also see Table 3. Elemental Analysis, calcd: C 42.79, H 2.96, N 5.87; found: C 40.47, H 3.09, N 5.95.

$[(\text{MeNNS})\text{Mn}(\text{CO})_3\text{Br}]$ (3_{CO}). Under inert atmosphere, 0.130 g (0.474 mmol) of $[\text{Mn}(\text{CO})_5\text{Br}]$ is stirred in 15 mL of CH_2Cl_2 in a round bottom flask until completely dissolved. Separately, 0.106 g (0.437 mmol) of MeNNS is diluted in 15 mL of CH_2Cl_2 . The ligand/ CH_2Cl_2 solution is added dropwise to the $[\text{Mn}(\text{CO})_5\text{Br}]$ solution. The mixture stirred overnight and there was a slow color change from yellow to dark red-brown. The solution precipitated some dark material and was filtered with a celite pipette to extract the fine precipitate from solution. The solution was placed into a Schlenk flask and placed in 4 °C which resulted in large red-orange blocks suitable for X-ray diffraction. Yield: 144 mg (72%). Selected IR bands (ν in cm^{-1} , ν_{CO} in italics): 2019 *m*, 1925 *vs*, 1618 *w* (ν_{CN}), 1579 *w*, 1263 *w*, 799 *m*, 626 *s*. UV/vis in CH_2Cl_2 , λ in nm (ϵ in $\text{cm}^{-1} \text{M}^{-1}$): 314 (7 490), 488 (1 530); also see Table 3. ^1H NMR in CD_2Cl_2 (δ from TMS): 8.46 *s* (1H), 7.91 *t* (1H), 7.76 *t* (2H), 7.52 *d* (1H), 7.39 *m* (2H), 7.31 *t* (1H), 3.13 *s* (3H), 2.53 *s* (3H). Elemental Analysis, calcd: C 44.27, H 3.06, N 6.07; found: C 43.94, H 3.12, N 6.00.

$[(\text{MeNNS})\text{Mn}(\text{Br})_2]$ (3_{Br}). **Method A.** A reaction was prepared according to the procedure for 3_{CO} stated above (3_{CO} collected as precipitate), and the filtrate was subjected to vapor diffusion

of Et₂O. This generated red crystals suitable for X-ray analysis. As the yield was <10%, we developed an alternative preparation. **Method B.** Under ambient atmosphere, 0.060 g (0.218 mmol) of [Mn(CO)₅Br] is stirred in 20 mL of CH₂Cl₂ in a round bottom flask until completely dissolved. Separately, 0.050 g (0.206 mmol) of MeNNS is diluted in 20 mL of Et₂O. The CH₂Cl₂ solution of the Mn carbonyl was distributed to a series of small test tubes. Next, the Et₂O solution of ligand was carefully layered on top of the Mn solution, and the mixture was capped and allowed to diffuse slowly for 1 week. This procedure afforded large red diamond shaped crystals suitable for X-ray diffraction. Yield: 27 mg (29%). Selected IR bands (ν in cm⁻¹, ν_{CO} in italics): 1586 m (ν_{CN}), 1378 m, 962 m, 794 s, 766 s, 738 s, 579 m. Magnetic moment (solid state, 298 K): $\mu_{\text{eff}} = 4.9 \mu_{\text{B}}$. Elemental Analysis, calcd: C 36.79, H 3.09, N 6.13; found: C 36.78, H 3.05, N 6.02.

[(N_{Me}NS)Mn(CO)₂Br] (4_{CO}). Under inert atmosphere, 0.146 g (0.531 mmol) of [Mn(CO)₅Br] was stirred in 10 mL of CH₂Cl₂ in a round bottom flask until completely dissolved. Separately, 0.108 g (0.446 mmol) of N_{Me}NS is diluted in 10 mL of CH₂Cl₂. The ligand/CH₂Cl₂ solution is added dropwise to the [Mn(CO)₅Br] solution. The mixture stirred overnight and there was a slow color change from yellow to dark red-orange. This red-orange solution was subjected to vapor diffusion of Et₂O at room temperature, which resulted in black needles suitable for X-ray diffraction. Yield: 152 mg (66%). Selected IR bands (ν in cm⁻¹, ν_{CO} in italics): 1918 s, 1847 s, 1594 w (ν_{CN}), 1430 m, 1256 w, 965 m. ¹H NMR in CD₂Cl₂: see main text. UV/vis in CH₂Cl₂, λ in nm (ϵ in cm⁻¹ M⁻¹): 319 (7 450), 560 (510); also see Table 3. ¹H NMR in CD₂Cl₂ (δ from TMS): two species observed; see main text. Elemental Analysis, calcd: C 44.36, H 3.26, N 6.47; found: C 43.53, H 3.30, N 6.33.

Subspecies of FPhNNS : [$(\text{FPhNNS})\text{Mn}(\text{CO})_3\text{Br}$] ($\mathbf{5}_{\text{CO-a}}$) and [$(\text{FPhNNS})\text{Mn}(\text{CO})_2\text{Br}$] ($\mathbf{5}_{\text{CO-b}}$).

Under N_2 atmosphere, 0.113 g (0.411 mmol) of $[\text{Mn}(\text{CO})_5\text{Br}]$ is stirred in 10 mL of DCM in a round bottom flask until a clear yellow-orange solution is obtained. In a separate round bottom flask, 0.108 g (0.335 mmol) of FPhNNS ligand is dissolved in another 10 mL DCM to generate a yellow solution. The ligand/DCM solution is added dropwise to the $[\text{Mn}(\text{CO})_5\text{Br}]$ solution. The mixture stirred overnight and there was a slow color change from yellow to a dark maroon-red solution. The reaction was split into two equal portions. **Portion A.** The first dark solution was subjected to vapor diffusion of pentane at room temperature (12-24 h), which resulted in small red cubic crystals of $\mathbf{5}_{\text{CO-a}}$ (S unbound) suitable for X-ray diffraction. Yield: 68 mg (Yield: 44%). Selected IR bands (ν in cm^{-1} , ν_{CO} in italics): 2021 s, 1943 s, 1914 vs, 1603 w (ν_{CN}), 1423 m, 1224 s, 846 vs, 733 s, 545 m. UV/vis in CH_2Cl_2 , λ in nm (ϵ in $\text{cm}^{-1} \text{M}^{-1}$): 497 (1 120). Elemental Analysis, calcd: C 48.82, H 2.79, N 5.18; found: C 48.67, H 2.70, N 5.21. **Portion B.** To the second portion of the reaction solution: slow vapor diffusion of Et_2O (1 to 3 days) afforded black needles of $\mathbf{5}_{\text{CO-b}}$ (S bound) suitable for X-ray diffraction. Yield: 73 mg (Yield: 46%). Selected IR bands (ν in cm^{-1} , ν_{CO} in italics): 1934 s, 1872 vs, 1607 m (ν_{CN}), 1474 s, 1171 s, 839 w, 749 vs, 519 w. UV/vis in CH_2Cl_2 , λ in nm (ϵ in $\text{cm}^{-1} \text{M}^{-1}$): 332 (3 250), 612 (495); also see Table 3. Elemental Analysis, calcd: C 49.14, H 2.95, N 5.46; found: C 48.84, H 2.82, N 5.47.

Physical Measurements. ^1H NMR spectra of ligands were collected on Varian DirecDrive 400 MHz spectrometer and chemical shifts were referenced to TMS. ^1H NMR spectra of the manganese complexes were recorded on a 500 MHz Varian Inova instrument fitted with a variable temperature apparatus. UV/vis absorption spectra were obtained using an Ocean Optics USB2000+XRS-ES detector probed with a PX2 pulsed xenon lamp. Solutions of the complexes

were prepared at ~0.1 mM in 1 cm quartz cuvettes in an argon drybox, and absorbances were measured with the aid of fiber optic feedthroughs. Infrared spectra of complexes in the solid state were recorded under ambient atmosphere on a Bruker Alpha spectrometer equipped with a diamond ATR crystal. The solid state magnetic moment of $\mathbf{3}_{\text{Br}}$ was determined using a Johnson-Mathey magnetic susceptibility balance.

X-ray Diffraction Data Collection and Crystal Structure Refinement. The data were collected on either a Rigaku AFC12 diffractometer with a Saturn 724+ CCD or on a Nonius Kappa CCD diffractometer using a Bruker AXS Apex II detector, both using a graphite monochromator with MoK α radiation. Reduced temperatures were maintained using an Oxford Cryostream low temperature device. Data reduction were performed using the Rigaku Americas Corporation's Crystal Clear version 1.40.2. Structures were solved by direct methods using SIR973 and refined by full-matrix least-squares on F^2 with anisotropic displacement parameters for the non-H atoms using SHELXL-97.4. Structure analysis was aided by use of the programs PLATON985 and WinGX.6. The hydrogen atoms on carbon were calculated in ideal positions with isotropic displacement parameters set to $1.2 \times U_{\text{eq}}$ of the attached atom ($1.5 \times U_{\text{eq}}$ for methyl hydrogen atoms). For $\mathbf{5}_{\text{CO-b}}$, a large peak persisted in the difference electron density map 2.4 Å from Mn. Additional but much smaller peaks were observed near Br1. These peaks were interpreted to be from a five coordinate Mn complex with one Br atom and one carbonyl group present in small quantities within the crystal. As such, the structure was modeled as a disordered species where the lone carbonyl group resides near the Br atom of the six coordinate species. The Br atom of the five coordinate species resides between the two carbonyl groups of the six coordinate complex. The relative occupancies of the two species were estimated by assigning the

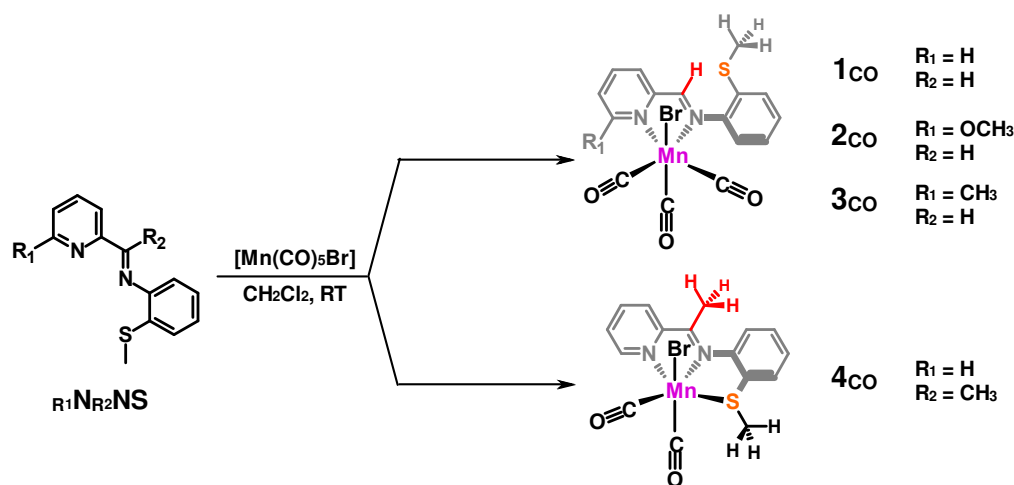
variable x to the site occupancy for Br1 and $(1-x)$ to the site occupancy for Br1a. A common isotropic displacement parameter was refined for the two Br atoms while refining the variable x . In this way, the site occupancy for Br1 refined to 96(1)%. The ratio of the six coordinate species in the crystal to the five coordinate species is 24:1. After an initial refinement, the coordinates for O1a and C2a were fixed along with their displacement parameters in the final refinement model.

Results and Discussion

Syntheses. The **NNS** ligands derived from aldehyde starting materials (denoted $R_1\text{NNS}$) were prepared under reported conditions (condensation in MeOH).²⁷⁻²⁸ The novel iminomethyl-substituted ligands (ketone starting materials; denoted $R_1\text{N}_{\text{Me}}\text{NS}$) were prepared by a zinc-templated reaction (AcOH, ZnCl₂, reflux) with 2-(methylthio)aniline. The resulting zinc-bound intermediate was de-metalated by treatment with aqueous oxalate, allowing extraction of the free ligand into the organic layer.

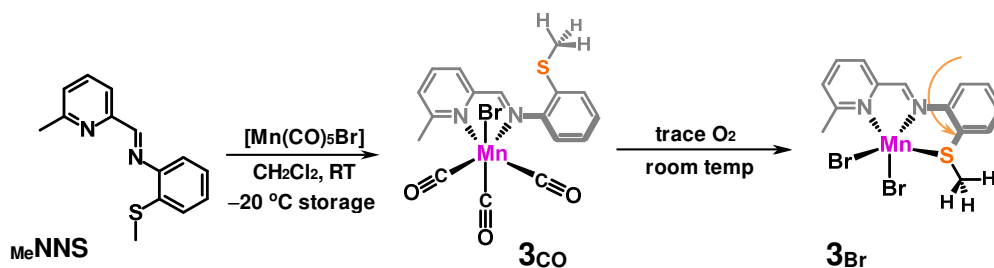
We pursued the metalation of **NNS**-type ligands with [Mn(CO)₅Br] under reported conditions (CH₂Cl₂, room temperature, N₂ atmosphere).¹⁷⁻²³ In general, the reaction of a yellow solutions of **NNS** and [Mn(CO)₅Br] generated a dark red color over the course of 15 min to 1 hour. Vapor diffusion of pentane or Et₂O afforded crystalline material that ranged from black to translucent orange. We found that ligation of the thioether-S donor was dependent on the nature of the Schiff base R-group. As shown in Scheme 1, metalations of aldehyde-derived ligands afford the **NNS** bound complex of type [(**RNNS**)Mn(CO)₃Br]. Coincidentally, the same reaction was reported by Mascharak and co-workers during preparation of this manuscript using the same **NNS** ligand, as well as its quinoline congener.²³ This trend of the unbound thioether-S is largely independent of the R-group at the *ortho* position of the pyridine moiety (H, CH₃, OCH₃). Conversely, substitution of a methyl group at the Schiff base affords the fully ligated complex [(**N_{Me}NS**)Mn(CO)₂Br]. Binding of the thioether is likely encouraged by steric repulsion between the Schiff base -CH₃ group and the aryl(methyl)thioether unit in the *S*-unbound state (vide infra, X-ray section). This trend is altered in the case of the hypermethylated ligand $\text{MeN}_{\text{Me}}\text{NS}$, wherein a five-coordinate species is obtained. The out-of-plane twisting induced by having both $R_1 = R_2$

= CH₃ (see X-ray section) and positioning of the thioether-S close to (but not at) an apical coordination site is likely responsible for exclusion of a sixth ligand.



Scheme 1. Metalation of substituted NNS ligands with [Mn(CO)₅Br];
the coordination mode is dependent on R₂.

The manganese carbonyls are generally stable in CH₂Cl₂ solution at 298 K under N₂, even in presence of trace amounts of O₂. One exception is the 2-methylpyridine complex [(Me₂NNS)Mn(CO)₃Br], which crystallized in sufficient purity only at -20 °C. At ambient temperature (and with trace O₂), this complex transforms to the Mn(II) dibromide complex [(Me₂NNS)Mn(Br)₂], in which the chelate is fully ligated.



Scheme 2. Metalation of MeNNS with [Mn(CO)₅Br] to form [(MeNNS)Mn(CO)₃Br] (**3Co**) and subsequent conversion to the Mn(II) dibromide species [(MeNNS)Mn(Br)₂] (**3Br**).

[see Table 1 in Attached Document]

Table 2. Selected bond distances (Å) and bond angles (deg).

R₁, R₂	1_{CO*} H, H	2_{CO} OCH ₃ , H	3_{CO} CH ₃ , H	3_{Br} CH ₃ , H	4_{CO} H, CH ₃	5_{CO-a} FPh, H	5_{CO-b} FPh, H
Mn–N_{py}	2.054(2)	2.0844(15)	2.097(2)	2.246(8)	1.987(2)	2.0954(16)	2.100(4)
Mn–N_{SB}	2.049(2)	2.0446(15)	2.045(2)	2.245(8)	2.029(2)	2.0488(16)	2.016(4)
Mn–S_{Me}	–	–	–	2.645(3)	2.3001(8)	–	2.3069(14)
Mn–Br	2.5338(5)	2.5216(3)	2.5314(5)	2.4877(18)	2.5564(7)	2.5250(4)	2.5690(10)
Mn–Br	–	–	–	2.4781(19)	–	–	–
Mn–C(O) trans SB	1.806(3)	1.815(2)	1.809(3)	–	1.789(3)	1.824(2)	1.805(5)
(Mn)C–O trans SB	1.148(3)	1.140(2)	1.139(4)	–	1.155(3)	1.144(2)	1.145(5)
Mn–C(O) trans Br	1.781(4)	1.798(2)	1.803(3)	–	1.789(3)	1.802(2)	1.799(4)
(Mn)C–O trans Br	1.148(4)	1.126(3)	1.143(3)	–	1.131(3)	1.132(3)	1.135(5)
Mn–C(O) trans py	1.802(3)	1.810(2)	1.811(3)	–	–	1.799(2)	–
(Mn)C–O trans py	1.148(3)	1.140(3)	1.142(4)	–	–	1.147(2)	–
Aryl-(SMe) Dihedral	65.92	70.00	68.46	9.33	31.92	64.64	5.18
S•••C(O)_{Br}	3.900	3.338	3.258	–	–	4.128	–
R₁•••C(O)_{SB}	2.646	2.666	~2.65	–	2.694	2.947	3.097

*values taken from reference 23

X-ray Structure

[(HNNS)Mn(CO)₃(Br)] (1_{CO}). During the course of this work, the X-ray structure of **1_{CO}** was reported by another research group.²³ For the purpose of comparison to the other complexes, we briefly describe the metrics of the reported complex here. Similar to **2_{CO}** (Fig. 1), the manganese center in **1_{CO}** is overall pseudo-octahedral, with the two N donors of the ligand bound to the metal center. The Mn–N_{py} and Mn–N_{SB} bond distances [2.054(2) and 2.049(2) Å, respectively] are typical for low-spin, Mn(I) nitrogen bonds in complexes bearing the 2-iminomethene-pyridyl moiety. The thioether-S is not bound to the manganese center, with the aryl(thioether) moiety rotated at a dihedral angle of 65.9° away from the planar pyridyl/Schiff base moiety. Because this distorts the otherwise planar, conjugated π-system of the ligand frame, this indicates a strong preference of the Mn(I) center for the back-bonding CO ligand versus the σ-donor only character of the thioether-S. There is, however, a somewhat close contact between the unbound S donor and the adjacent carbonyl – the S•••C(O) distance is ~3.9 Å. The three carbonyl ligands are bound in a facial arrangement (as nearly always found in tricarbonyls), and exhibit Mn–C(O) distances of 1.806(3), 1.781(4), 1.802(3) Å – the shortest of which is bound trans to the Br[–] ion. The Mn–Br distance of 2.5338(5) Å is predictably long due to repulsion between the low-valent Mn(I) and bromide ion, and in a similar range to other Mn(I) carbonyl bromides.

[(OMeNNS)Mn(CO)₃(Br)] (2_{CO}). The X-ray structure of the methoxy-appended complex **2_{CO}** is also shown in Fig. 1. Overall, the complex exhibits similarity to **1_{CO}** in that the coordination geometry is pseudo-octahedral and the thioether moiety remains unbound; the three carbonyl ligands are also arranged in the same facially coordinating fashion. The Mn–N_{py} bond distance of 2.0844(15) Å is slightly longer than that found in **1_{CO}** (Mn–N_{py} = 2.054(2) Å), likely due to the steric repulsion due to the ortho methoxy group. The repulsion effect is not apparent in the

Mn–N_{SB} bond distances found in **2**_{CO} [2.0446(15) Å] and **1**_{CO} (2.049(2) Å]. The methoxy-O donor is located 3.207 Å away from the Mn center, distinctly outside the range of normal Mn–O bonding. Notably, the distance between the methoxy-O and the C-donor of the adjacent carbonyl is quite short – only 2.66 Å. As found in **1**_{CO}, there is a subtle interaction between the unbound thioether and a carbonyl ligand. This interaction appears to be more pronounced in the case of **2**_{CO} [S...C(O) ≈ 3.34 Å] versus that observed in **1**_{CO} [S...C(O) ≈ 3.9 Å]. This appears to occur in **2**_{CO} due to a slightly greater twist of the aryl(methyl)thioether moiety (70.0°) versus that in **1**_{CO} (65.9°). Interestingly, the largest differences in carbonyl ligand metrics between **2**_{CO} and **1**_{CO} occur at the carbonyl participating in the interaction with the thioether S moiety. While the Mn–C–O bond angles are nearly invariant in each complex [174.03(18)°, 174.86(16)°], in **2**_{CO} the Mn–C(O) and (Mn)C–O bonds [1.798(2), 1.126(3) Å] are significantly longer than the same distances in **1**_{CO} [1.781(4), 1.148(4) Å]. This suggests the S...C(O) interaction is significant, and generates weaker bonding along the Mn–C–O axis due to partial donation of sulfur lone pair to the Lewis acidic carbonyl C. The remaining bond distances to the carbonyl and bromide ligands are unremarkable.

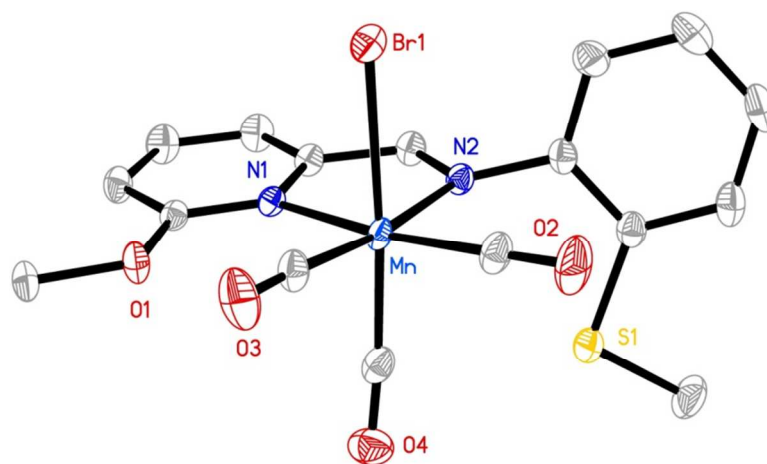


Fig. 1. ORTEP diagram (50% ellipsoids) of [(OMeNNS)Mn(CO)₃Br] (**2**_{CO}).

H atoms are omitted for clarity.

$[(\text{MeNNS})\text{Mn}(\text{CO})_3(\text{Br})]$ ($\mathbf{3}_{\text{CO}}$). The X-ray structure of the 2-methylpyridine derived manganese carbonyl $\mathbf{3}_{\text{CO}}$ is shown below in Fig. 2. This manganese species exhibits a similar binding mode and overall coordination geometry to $\mathbf{1}_{\text{CO}}$ and $\mathbf{2}_{\text{CO}}$. The steric effect of the 2-methyl group at the pyridine moiety is quite pronounced, resulting in a long Mn–N_{py} bond of 2.097(2) Å, versus the corresponding Mn–N_{py} distance of 2.0844(15) Å and 2.054(2) Å in $\mathbf{2}_{\text{CO}}$ and $\mathbf{1}_{\text{CO}}$, respectively. However the Schiff base N-donor remains bound at approximately the same distance (2.045(2) Å) as found in $\mathbf{1}_{\text{CO}}$ and $\mathbf{2}_{\text{CO}}$. And although the –CH₃ protons were not experimentally located in the diffraction map, the model suggests that the CH₃•••C(O) distance is short – in the range of 2.6 to 2.7 Å – and less than the sum of the Van der Waals radii (~2.8 Å). However, there is no resulting perturbation of the Mn–C–O bond metrics in $\mathbf{3}_{\text{CO}}$ versus $\mathbf{2}_{\text{CO}}$ or $\mathbf{1}_{\text{CO}}$ that can be attributed to the infringing methyl unit. Interestingly, in $\mathbf{3}_{\text{CO}}$ the S•••C(O) interaction (~3.26 Å) is closer than in $\mathbf{2}_{\text{CO}}$ or $\mathbf{1}_{\text{CO}}$, but unlike $\mathbf{2}_{\text{CO}}$ there is no significant change in Mn–C–O bond metrics versus $\mathbf{1}_{\text{CO}}$. The remaining Mn–C(O), C–O and Mn–Br distances are listed in Table 2.

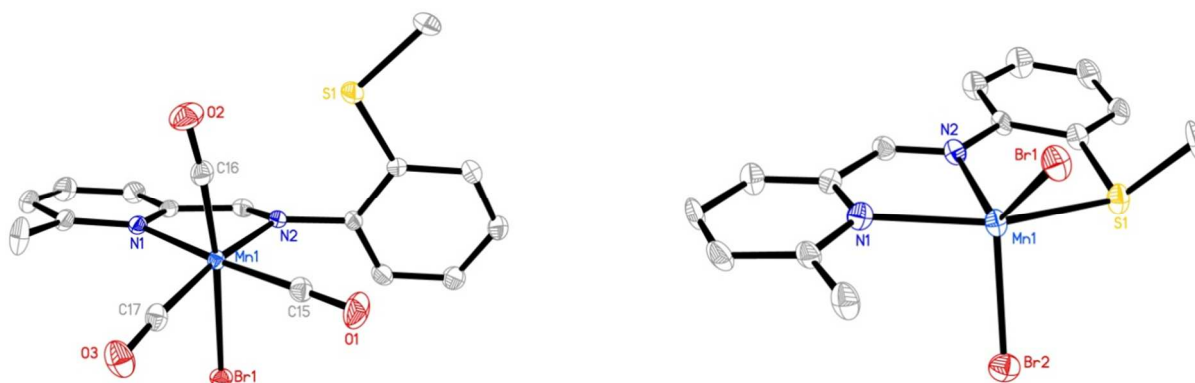


Fig. 2. ORTEP diagrams of the molecular structures of $[(\text{MeNNS})\text{Mn}(\text{CO})_3\text{Br}]$ ($\mathbf{3}_{\text{CO}}$, 50% ellipsoids) and $[(\text{MeNNS})\text{Mn}(\text{Br})_2]$ ($\mathbf{3}_{\text{Br}}$, 30% ellipsoids). H atoms are omitted for clarity.

[(MeNNS)Mn(Br)₂] (3_{Br}). The X-ray structure of the dibromide complex [(MeNNS)Mn(Br)₂] is shown in Fig. 2 (right side). Both the Mn–N [2.246(8), 2.245(8) Å] and Mn–Br [2.4877(18), 2.4881(19) Å] bond distances found in **3_{Br}** are longer than in the corresponding manganese carbonyl, due to the high-spin configuration of the complex (vide infra, Spectroscopy section). Of note is the fact that this complex is monomeric; many dihalide complexes of Mn(II) with bidentate or tridentate ligands exhibit a dimeric motif via a μ -(X)₂ (where X = Cl, Br) bridge. It is likely that dimerization is prevented by the combined steric effects of the 2-methylpyridine and thioether S–CH₃ units. Close inspection of the structural database reveals numerous examples of dimerized Mn₂Br₂ complexes.^{29–33} However, the arrangement of the capping ligands is always parallel and close-packed – a configuration not possible with the two pendant methyl units (-SCH₃ and ortho_{py}-CH₃).

[(NMeNS)Mn(CO)₂(Br)] (4_{CO}). The tridentate NNS ligand bearing a methyl substituent at the Schiff base linkage in **4_{CO}** is fully ligated in NNS fashion to the manganese center (Fig. 3). As a result, the Mn–N_{py} and Mn–N_{SB} bonds in **4_{CO}** are much shorter (1.982(2) and 2.029(2) Å, respectively) than those in **1_{CO}**, presumably due to the chelation effect of all three bound donor atoms. The Mn–S bond distance of 2.301(8) Å is similar to that found in the only other mixed N/S(thioether) manganese carbonyl [2.3449(6), 2.3467(7) Å].²⁶ The Mn–S bond length in **4_{CO}** is also much shorter than in the Mn(II) dibromide species described herein [**2_{Br}**, 2.6839(13); **3_{Br}**, 2.645(3) Å]. Interestingly, binding of the thioether-S induces a twist in the conjugated ligand frame, exhibiting a dihedral angle of 32.06° from the Schiff base to the aryl(thioether) moiety. In **4_{CO}**, the origin of thioether ligation is likely steric: In **1_{CO}**, the distance from the unbound and 'twisted' aryl–S–CH₃ to the imine-H is ~3.0 Å. In the case of **4_{CO}**, replacement of the imine-H

with imine-CH₃ would decrease this contact to within the Van der Waals radii, disallowing protrusion of the thioether in the direction of the Schiff base linkage. Thus, binding of the S-donor and concomitant release of one carbonyl ligand is preferred in **4**_{CO}. The two remaining carbonyl ligands are bound in *cis* fashion (Mn–C(O) = 1.789(3), 1.789(3) Å), as is obligatory in manganese dicarbonyls. The remaining coordination site is occupied by bromide at a distance of 2.5564(7) Å.

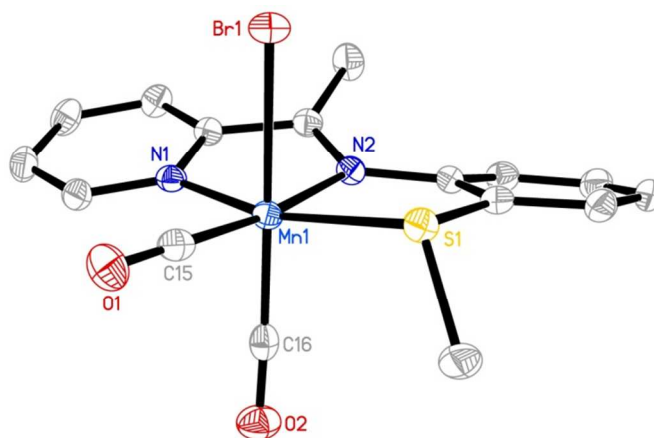


Figure 3. ORTEP diagram (50% ellipsoids) of the molecular structure of [(N_{Me}NS)Mn(CO)₂Br] (left, **4**_{CO}). H atoms are omitted for clarity.

Spectroscopic Characterization

Infrared Spectra. The IR spectrum of [(HNNS)Mn(CO)₃Br] (**1**_{CO}) is shown in Fig. 4 (bottom red line), wherein the carbonyl stretches at 2023, 1917, and 1867 cm⁻¹ are due to the three chemically distinct carbonyls in the complex. Comparison of this IR with that of the fully ligated dicarbonyl complex [(N_{Me}NS)Mn(CO)₂Br] (**4**_{CO}) allows identification of the highest energy (and lowest intensity) peak at 2023 cm⁻¹ in **1**_{CO} as the CO ligand trans from the N_{py} donor (absent in **4**_{CO}). The high energy of this stretch is presumably due to the strong π-acceptor capacity of the pyridine moiety. In the same vein, we assign the lowest energy ν(CO) stretches (1867 cm⁻¹ in

1_{CO}; 1847 cm⁻¹ in **4**_{CO}) as the carbonyl ligand trans from the Br⁻ donor, due to its greater π -donor strength (greater $\pi^*(\text{CO})$ electron density). The remaining $\nu(\text{CO})$ stretches are of nearly identical value (1917 cm⁻¹, **1**_{CO}; 1918 cm⁻¹, **4**_{CO}; 1918 cm⁻¹, **5**_{CO}), owing to their analogous chemical environment trans from the N_{SB} donor. The other tricarbonyls (**2**_{CO}, **3**_{CO}) follow the same trend. The IR spectrum of the 2-methylpyridine species **3**_{CO} is shown at the bottom of Fig. 4. Although it is a tricarbonyl like **1**_{CO}, the spectrum of **3**_{CO} does not exhibit three distinct $\nu(\text{CO})$ bands. Rather, the two lower energy stretches (assigned as trans to Br, and trans to N_{SB}) appear largely merged near 1925 cm⁻¹. The steric (or agostic) perturbation of the CO ligands' environment(s) by the ortho methyl group is thus apparent. Overall, due to the varying coordination geometries, we unambiguously assigned each CO stretch. Future complexes could be structurally assigned on this basis (IR) in the absence of X-ray structural characterization.

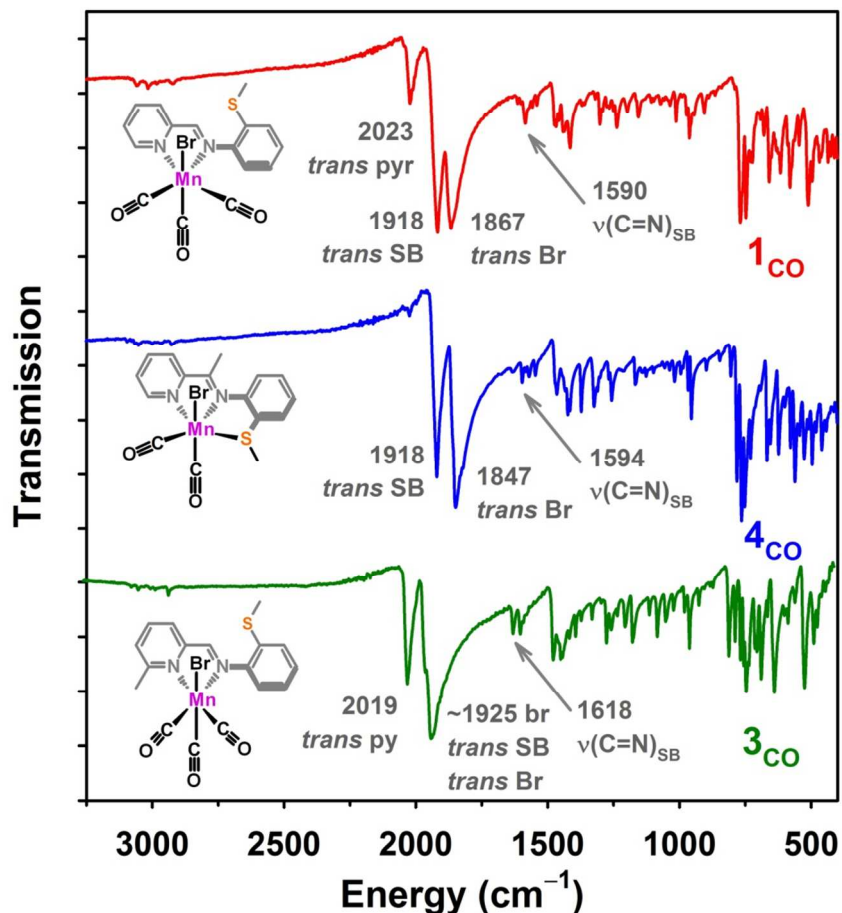


Fig. 4. Infrared spectra of [(H_LNNS)Mn(CO)₃Br] (**1_{CO}**, top red line), [(N_{Me}NS)Mn(CO)₂Br] (**4_{CO}**, middle blue line) and [(MeNNS)Mn(CO)₃Br] (**3_{CO}**, bottom green line) at 298 K in the solid state.

¹H NMR Spectra of 1_{CO}, 3_{CO} and 4_{CO}. This set of complexes represents all of the structural motifs found in the X-ray structures reported in this work. The properties of several complexes in CD₂Cl₂ solution were investigated with regard to the bound/unbound thioether unit. We found that two complexes (**1_{CO}**, **3_{CO}**) exhibited ¹H NMR spectra consistent with a single species in solution (according to their X-ray structure), whereas one complex (**4_{CO}**) exhibited two species in solution. Below we discuss the straightforward cases of **1_{CO}** and **3_{CO}**, followed by a comparative interpretation of the more complex phenomena observed for **4_{CO}**.

The ^1H NMR spectrum of $\mathbf{1}_{\text{CO}}$ in CD_2Cl_2 at room temperature is shown in Fig. 5. The broadness of the peaks and lack of observed multiplicities was not resolved by lower temperature spectra (see Supporting Information, Fig. S1). Nonetheless, the spectrum indicates the presence of a single species in solution, and the unbound state of the thioether-S is indicated by the nearly unchanged value of the S- CH_3 peak in the complex (2.54 ppm) versus that of the free NNS ligand (2.48 ppm). The furthest downfield peaks are indicative of the imino N=C(H) (9.27 ppm) in $\mathbf{1}_{\text{CO}}$, which is shifted significantly downfield from the free ligand ($\delta_{\text{free}} = 8.57$ ppm). This claim is supported by the spectrum of the iminomethyl complex $\mathbf{4}_{\text{CO}}$ (vide infra), which exhibits no Schiff base H (singlet) in the 8.5-9.5 ppm region. The C- H at the ortho position of the bound pyridine experiences a smaller downfield shift upon metal binding ($\delta_{\text{bound}} = 8.99$ ppm; $\delta_{\text{free}} = 8.70$). This claim is supported by the spectrum of the ortho-methylpyridine complex $\mathbf{3}_{\text{CO}}$ (vide infra), which exhibits no ortho H_{py} (doublet) peak near between ~ 8.5 and 9.0 ppm.

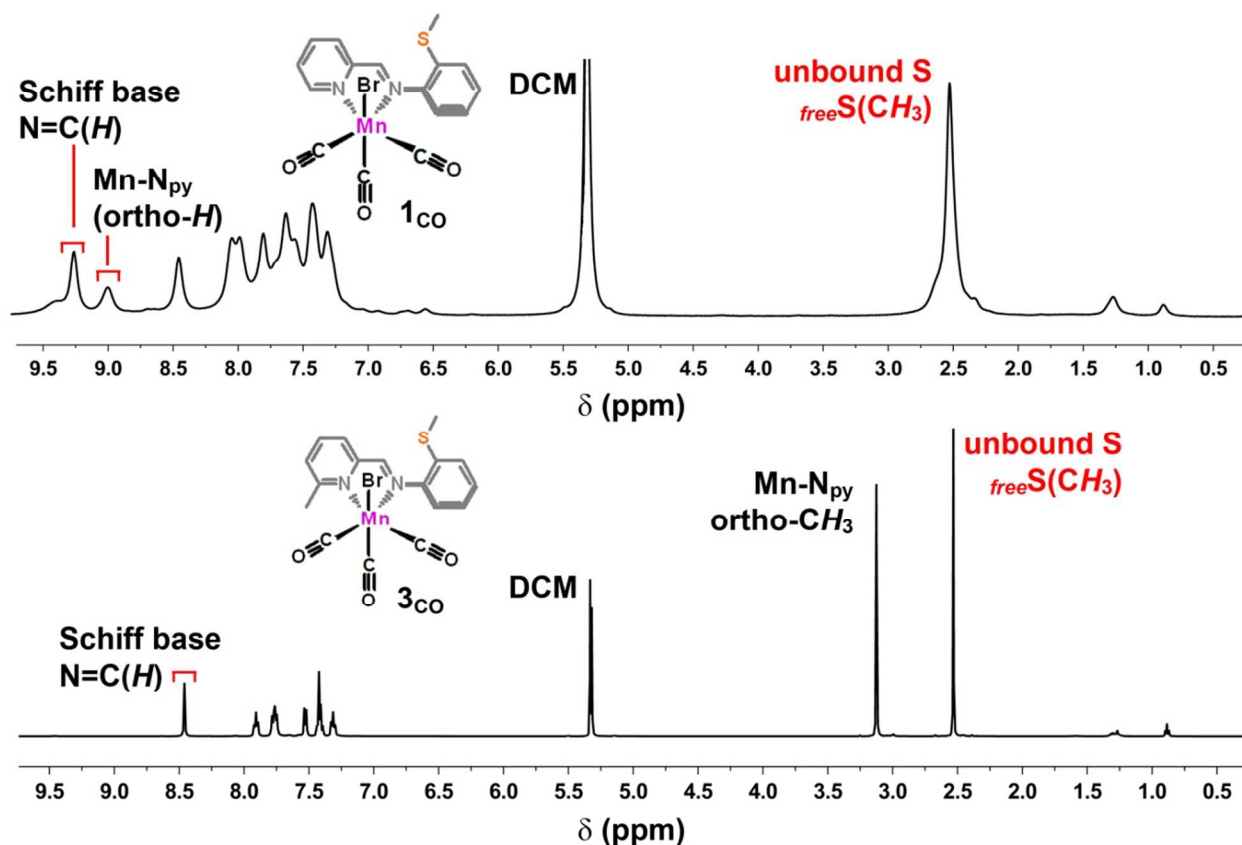


Fig. 5. ^1H NMR spectra (500 MHz) of $[(\text{NNS})\text{Mn}(\text{CO})_3\text{Br}]$ (1_{CO} , top panel) and $[(\text{MeNNS})\text{Mn}(\text{CO})_3\text{Br}]$ (3_{CO} , bottom panel) in CD_2Cl_2 at 25°C .

The ^1H NMR spectra of $[(\text{MeNNS})\text{Mn}(\text{CO})_3\text{Br}]$ (3_{CO}) in CD_2Cl_2 is shown at the bottom of Fig. 5. This complex exhibits a much sharper spectrum at ambient temperature, and is broadened by VT experiments at lower temperature (Supporting Information, Fig. S2). This complex exhibits a $\text{N}=\text{C}(\text{H})$ resonance at 8.46 ppm, which is quite similar compared to the free MeNNS ligand ($\delta_{\text{free}} = 8.55$ ppm). In the alkyl region, the complex exhibits two resonances (each 3H, singlet) corresponding to the $\text{S}-\text{CH}_3$ and $o\text{-CH}_3(\text{py})$ units. These peaks are not readily assigned in the spectrum of the free ligand (2.63, 2.47 ppm; 3H, singlets) due to their proximity. As the pyridine unit is bound to the Mn center in all structurally characterized complexes, we ascribe the downfield-shifted resonance at 3.13 ppm to the Mn-bound ortho $\text{CH}_3(\text{py})$ unit. We do not ascribe this resonance to the $\text{S}-\text{CH}_3$ unit (instead ascribed to the feature at 2.53 ppm), as only a Mn-

bound thioether unit would exhibit a feature near ~ 3 ppm (vide infra). The X-ray structure of **3**_{CO} (Fig. 2) also strongly argues against thioether-S binding in solution (crystallized from CH₂Cl₂, NMR studies performed in CD₂Cl₂). In contrast, we do present evidence of thioether-S binding in the case of **4**_{CO} (vide infra), which does exhibit a Mn-bound thioether unit in the X-ray structure.

The ¹H NMR spectra of [(N_MeNS)Mn(CO)₂Br] (**4**_{CO}) is shown in Fig. 6. The room temperature spectrum of **4**_{CO} (top) exhibits broad peaks devoid of observable multiplicities. The resonance peaks become somewhat sharper upon decreasing the temperature from RT \rightarrow -40 °C. However, no changes in the number of peaks nor chemical shifts are observed. Below -40 °C (not shown), the peaks revert to broader linewidths due to the limited solubility of **4**_{CO} in CD₂Cl₂. As envisaged from the X-ray structure of **4**_{CO} (thioether-S bound), the complex should exhibit two resonances in the alkyl region, emanating from *i*) the N=C(CH₃) unit (2.34 ppm in the free ligand), and *ii*) the thioether moiety ($\delta_{\text{free}} = 2.43$ ppm); however, four peaks are observed in this region. Similarly, a set of eight resonances are expected in the aromatic region, but a more complicated set of >10 peaks is observed. One readily identifiable aromatic feature(s) should be the ortho-*H* of the bound pyridine, observed near ~ 9 ppm. Two broad peaks are observed in this region (9.29, 8.98 ppm) in a 1.3:1 ratio. This suggested that two species were present in solutions of **4**_{CO} in CD₂Cl₂.

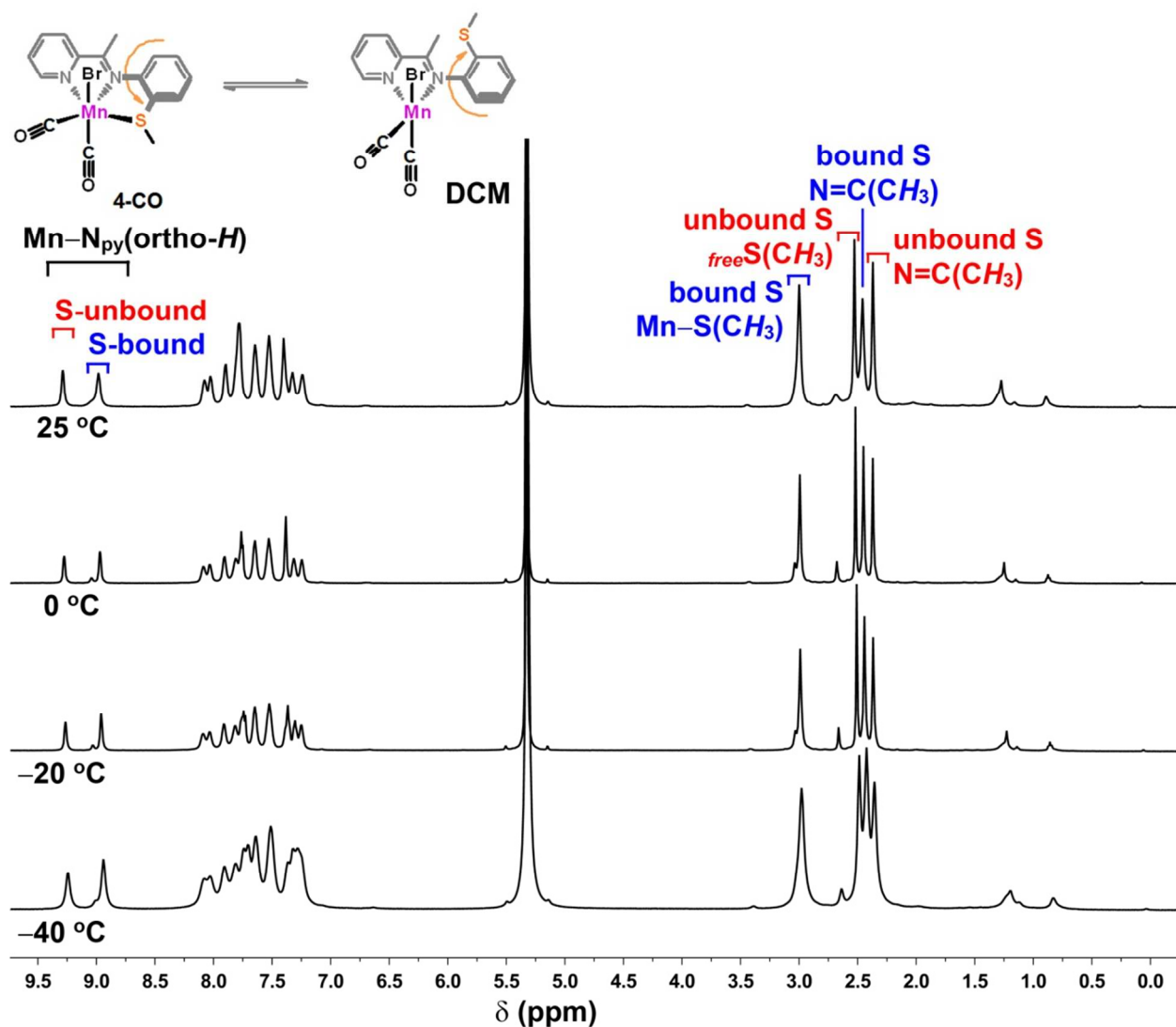
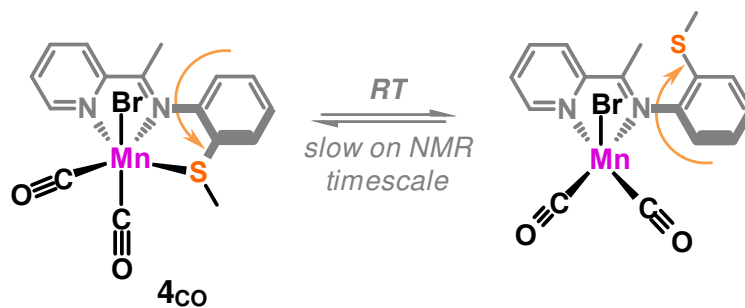


Fig. 6. Variable temperature ^1H NMR spectra (500 MHz) of solution species derived from dissolving crystals of $[(\text{N}_{\text{Me}}\text{NS})\text{Mn}(\text{CO})_2\text{Br}]$ (4_{CO}) in CD_2Cl_2 .

Overall, integration of the spectrum of 4_{CO} at $-20\text{ }^\circ\text{C}$ (optimum resolution) reveals that the two distinct sets of peaks are present in a roughly 1.3:1 ratio; the ratio is temperature independent in the accessible range ($\text{RT} \rightarrow -40\text{ }^\circ\text{C}$). In the alkyl region, the furthest downfield methyl resonance at 3.01 ppm is significantly different than the furthest downfield resonance in the free ligand (2.43 ppm). Based on the X-ray structure of 4_{CO} that exhibits a Mn-bound thioether-S, we assign the peak at 3.01 ppm as the Mn-bound S- CH_3 unit. By integration, the corresponding

Schiff base (N=C)CH₃ unit is observed at 2.47 ppm. The furthest upfield peak in the spectrum of **4**_{CO} (2.39 ppm) is quite similar to the Schiff base methyl peak in the free ligand (2.34 ppm), and we assign it as the (N=C)CH₃ unit in a second species. As the one remaining alkyl resonance at 2.54 ppm is quite similar to that of the unbound thioether in the free ligand (2.43), we assign it as belonging to this second species in solution in which the thioether-S is unbound. Based on integration values, we assign the peak at 8.98 to the S-bound (S trans to py) species and the 9.29 feature to the S-unbound species (CO trans to py). Due to lack of observable multiplicities, the assignment of the remaining aromatic peaks remains ambiguous.



Scheme 3. Speciation observed between diamagnetic 6- and 5-coordinate species as observed in the case of **4**_{CO} in ¹H NMR experiments in CD₂Cl₂.

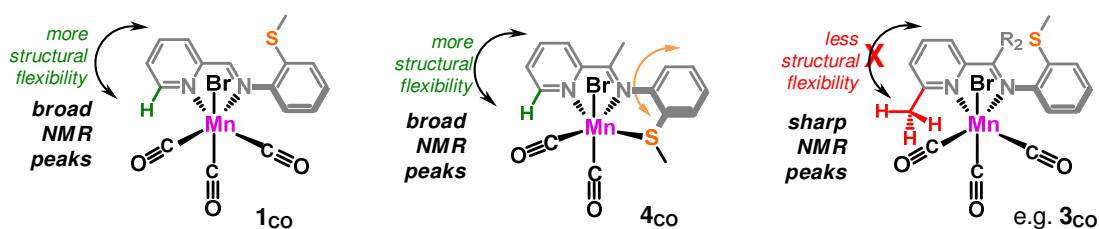
We hypothesized that the second species in solution (i.e. "S-unbound", not crystallographically characterized) was the five-coordinate species as shown above in Scheme 3. To our knowledge, there are three authentic precedents (i.e. no redox active ligand) regarding the isolation and X-ray structural characterization of five-coordinate Mn(I) carbonyls; all are deep blue, diamagnetic species supported by P₄ phosphine donor sets (2 × dppe, depe, etc.) in rigid square pyramidal orientation.³⁴⁻³⁶ The ¹H NMR experiments described above (~10-100 mM concentrations) indicated that the relative proportions of the two populations were not affected by temperature (RT → -40 °C). However, in the course of performing routine, analytical UV/vis measurements,

we noted a drastic change in color upon dilution of red solutions of **4**_{CO} to a blue/violet color. This indicated a possible change in relative proportions of species (5- and 6-coordinate) as a function of concentration.

The fact that the peaks do not coalesce at any tested temperature indicates that the kinetics of the equilibrium do not occur on the NMR timescale. This is not surprising in light of the low-spin, d^6 kinetically inert configuration of the pseudo-octahedral manganese center, which would prevent rapid interconversion between conformers. The octahedral ligand field splitting would be amplified by the t_{2g} type interactions among the metal-carbonyl $\{d_p(\text{Mn})-\pi^*(\text{CO})\}$ bonding units. Thus, there are two distinct, kinetically stable populations of species during the NMR experiment in CD_2Cl_2 . The reason(s) for the preferential crystallization of the S-bound conformer from CH_2Cl_2 in the synthetic procedure is not clear at this time.

The observed broadness of the peaks in **1**_{CO} and **4**_{CO} is most likely due to the conformational flexibility of the unbound aryl-thioether unit. While the broad linewidths in the case of **4**_{CO} may be related to the slow interconversion of the two species (S-bound and S-unbound), the reason for the peak broadness in **1**_{CO} remains unclear. As a corollary, the reason for the structural rigidity in the case of **3**_{CO} (viz a vis sharp ¹H NMR spectra) also is not clear. It is possible that the ortho $\text{CH}_3(\text{py})$ unit serves as a structural "anchor" that fixes the ligand framework in position via an agostic interaction with the CO ligand trans to the N_{SB} donor. The interaction of the 2-methylpyridine moiety with the carbonyl ligand (i.e. $\text{pyCH}_3\cdots\text{C}\equiv\text{O}$) may account for the anomalously large downfield shift (~ 0.5 ppm) observed for the ortho $\text{CH}_3(\text{py})$ unit, which is 2 atoms away from the metal binding site. Note that by comparison, the Schiff base methyl unit

(also 2 atoms away from the metal binding N) exhibits an almost immeasurable shift (~ 0.1 ppm) upon ligation. As a third case in point, we observe that the *ortho*-CH₃ bearing **3**_{CO} exhibits unusually low solubility in CH₂Cl₂ solution as compared to all other complexes – even the unsubstituted **1**_{CO}, which would be expected to exhibit the lowest solubility. And although this might be an anecdotal coincidence, it may instead be related to its relative rigidity (or lack of conformational motion) in solution. Preliminary DFT calculations, however, did not reveal any orbital overlap or shared MO density between the *ortho* CH₃(py) unit and the carbonyl ligand.



Scheme 4. Schematic representation regarding the observed broad linewidths of **1**_{CO} and **4**_{CO} (but not **3**_{CO}) in ¹H NMR experiments in CD₂Cl₂.

S-Bound and -Unbound Conformers Derived from _{FPh}NNS

Lastly, we wished to determine the effect of a much larger substituent at the pyridine *ortho* position. Under identical reaction conditions, metalation of the fluorophenyl derived ligand _{FPh}NNS has led to structural characterization of both conformers (S bound / unbound). Fig. 7 below shows conclusively that the fluorophenyl ligand can support both binding modes. Red crystals (blocks) of the tricarbonyl complex **5**_{CO-a} (S unbound) were obtained by fast vapor diffusion of pentane (~ 12 h to 1 d) into the reaction mixture in CH₂Cl₂. Alternatively, crystallization of the same reaction mixture via slow vapor diffusion of Et₂O (2 to 3 days) afforded crystals of **5**_{CO-b} (black needles, S bound). The ¹H NMR spectrum of **5**_{CO-a} reveals a single species in solution over the course of one experiment (minutes to 1-2 hours).

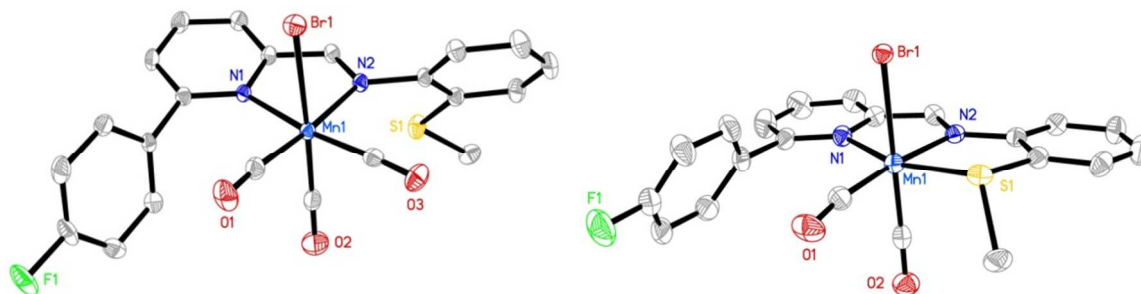
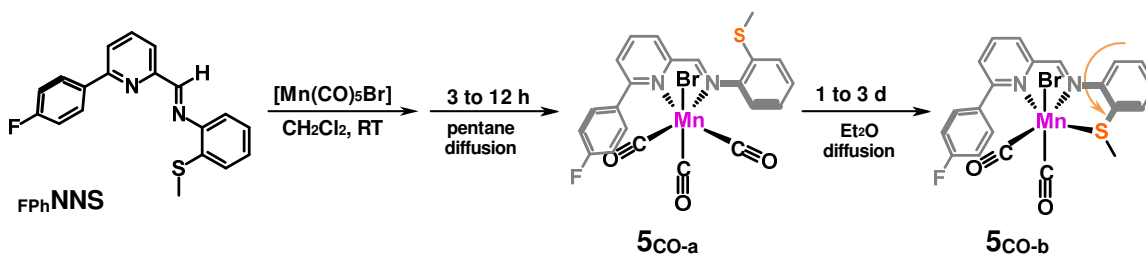


Fig. 7. ORTEP diagrams (50% ellipsoids) of the structural conformers of the FPhNNS ligand: $[(\text{FPhNNS})\text{Mn}(\text{CO})_3\text{Br}]$ ($\mathbf{5}_{\text{CO-a}}$, left) and $[(\text{FPhNNS})\text{Mn}(\text{CO})_2\text{Br}]$ ($\mathbf{5}_{\text{CO-b}}$, right). For a description of the full disorder model found for $\mathbf{5}_{\text{CO-b}}$, see X-ray section in Experimental and Supporting Information (Fig. S2).

The structural parameters of $\mathbf{5}_{\text{CO-a}}$ versus $\mathbf{5}_{\text{CO-b}}$ warrant several comments. In the S-unbound state $\mathbf{5}_{\text{CO-a}}$, the fluorophenyl unit is quite close to the proximal carbonyl: the ipso carbon (C14) is located at a distance of ~ 2.95 Å from the carbonyl (C20). This same carbonyl unit exhibits the longest Mn–C(O) distance (1.824(2) Å) of all of the complexes reported here, likely due to the close proximity of the fluorophenyl unit. The FPh unit is also twisted out of the conjugated plane by 62.1° , and even more strikingly it diverges 8° from the expected linear alignment across the $\text{C}_{\text{py}}\text{-C}_{\text{ipso}}\text{-C}_{\text{F}}$ axis. In contrast, the S-bound conformer $\mathbf{5}_{\text{CO-b}}$ exhibits a more 'relaxed' orientation of the fluorophenyl unit. The $\text{C}_{\text{ipso}}\cdots\text{C}(\text{O})$ distance is elongated to 3.097 Å, and the phenyl unit (although still twisted 62.8° out of the conjugated plane), adopts a more conventional, linear orientation along the $\text{C}_{\text{py}}\text{-C}_{\text{ipso}}\text{-C}_{\text{F}}$ axis (178.85°). The IR spectra of the complexes is also consistent with these findings. Complex $\mathbf{5}_{\text{CO-a}}$ (the tricarbonyl) exhibits three CO stretches at 2021, 1943 and 1914 cm^{-1} , while $\mathbf{5}_{\text{CO-b}}$ (dicarbonyl) exhibits two CO stretches at 1934 and 1872 cm^{-1} . These are also consistent with the $\nu(\text{CO})$ values for $\mathbf{1}_{\text{CO}}$ and $\mathbf{4}_{\text{CO}}$ depicted in Fig. 4.



Scheme 5. Preparation and sequential isolation of $[(\text{FPhNNS})\text{Mn}(\text{CO})_3\text{Br}]$ ($5_{\text{CO-a}}$) and $[(\text{FPhNNS})\text{Mn}(\text{CO})_2\text{Br}]$ ($5_{\text{CO-b}}$).

Electronic Absorption Spectra

In making routine UV/vis measurements, we noticed the blue or violet colors observed in dilute solutions of several of the complexes – namely 2_{CO} , 4_{CO} and $5_{\text{CO-b}}$ ($\lambda_{\text{abs}} = 611, 560, 612$ nm respectively); the dicarbonyls 4_{CO} and $5_{\text{CO-b}}$ crystallized as black crystals, which upon crushing in KBr afforded grayish-violet powders. [Note that 4_{CO} showed multiple species in ^1H NMR experiments.] In contrast, species exhibiting orange to red solutions were correlated with complexes that exhibited a single set of peaks in the ^1H NMR spectrum (1_{CO} , 3_{CO}). Table 3 summarizes the collected UV/vis data.

We hypothesize that the blue species observed with 4_{CO} in CH_2Cl_2 (where two species were observed in ^1H NMR, vide supra) may be the 5-coordinate species in which the thioether-S is unbound. There are several previous reports of 5-coordinate Mn(I) carbonyls that have been structurally characterized: $[(\text{PN}_{\text{Me}}\text{P})(\text{dppm})\text{Mn}(\text{CO})]^+$, $[(\text{dppe})_2\text{Mn}(\text{CO})]^+$ and $[(\text{depe})_2\text{Mn}(\text{CO})]^+$.³⁴⁻³⁶ Each complex was described as "dark blue" or "deep blue" by the reporting authors (no UV/vis data reported), both in solution and in crystalline form. It is possible that the blue species observed in this work under dilute conditions in non-coordinating solvent (dry CH_2Cl_2 , argon atmosphere) is also such a 5-coordinate species. It also is possible that at higher concentrations, $\text{Mn}\cdots\text{Mn}$ interactions or intermolecular $\text{Mn}\cdots\text{S}(\text{unbound})$

associations prevent accumulation of sufficient quantities of the 5-coordinate species. We are further investigating the nature of the blue species by more detailed spectroscopies and structural characterization attempts.

Table 3. UV/vis data (wavelengths in nm, ϵ -values in $M^{-1} cm^{-1}$) of manganese carbonyls as recorded in dry CH_2Cl_2 under argon atmosphere (298 K).

Complex	Color	λ_1 in nm (ϵ in $M^{-1} cm^{-1}$)	λ_2 in nm (ϵ in $M^{-1} cm^{-1}$)
1_{CO} [(NNS)Mn(CO) ₃ Br]	Orange	323 (20 000)	—
2_{CO} [(OMeNNS)Mn(CO) ₃ Br]	Blue	354 (4000)	611 (4000)
3_{CO} [(MeNNS)Mn(CO) ₃ Br]	Yellow	314 (7490)	488 (1570)
4_{CO} [(NMeNS)Mn(CO) ₂ Br]	Violet	319 (7450)	560 (800)
5_{COa} [(FPhNNS)Mn(CO) ₃ Br]	Red	325 (6 300)	497 (1120)
5_{COb} [(FPhNNS)Mn(CO) ₂ Br]	Teal	332 (3250)	612 (500)

— no peak observed in 550-650 nm region

Conclusion

Overall, the sequential fashion of the isolation of **5**_{CO-a} and **5**_{CO-b} (and structural characterization of both conformers), as well as ¹H NMR and UV/vis measurements allow us to postulate a step-wise scheme to explain all of the results observed herein. Metalation of [Mn(CO)₅Br] with NNS-type ligands affords an initial product wherein the ligand is bound in NNS fashion (S unbound). Depending on the nature of both R₁ and R₂, conversion to the S-bound species can be fast, slow or not observed. In the case of R₁, conversion of the tricarbonyl to the dicarbonyl is mildly accelerated by a large change in sterics. A very bulky R₁ substituent (i.e. for R₁ = FPh, but not CH₃ or OCH₃) induces a 'puckering' of the bound NNS fragment; this tension is released upon binding of the sulfur in the dicarbonyl. For R₂ (Schiff base substituent), conversion of the tricarbonyl to the dicarbonyl is accelerated by even a small steric change (R₂ = H→CH₃), due to steric repulsion of the S-CH₃ unit with N=C(CH₃) in the unbound state. This results in several examples of a {Mn(CO)₂} fragment supported by a neutral, thioether-containing ligand.

Summary

We summarize our findings in the following points:

- a) Consistent with others' findings, thioether-S donors are generally not favorable donors in manganese(I) carbonyl systems.
- b) Substitution of an iminomethyl moiety can enforce binding of the thioether-S, likely due to unfavorable steric interactions in the unbound conformation of the ligand.
- c) In the iminomethyl ligand ($N_{Me}NS$), 1H NMR studies reveal an equilibrium of the 6-coordinate (S bound) and a second [possibly 5-coordinate (S unbound)] species. The 1H NMR spectra of the aldehyde-derived NNS complexes reveal a single conformer – the S-unbound species.
- d) A significant electronic and steric substitution at the pyridine *ortho* position (fluorophenyl) leads to isolation of both S-bound and S-unbound species with resolution provided by kinetics (12 h versus 3 days crystallization time) and/or choice of crystallization solvent (pentane vs Et_2O).
- e) We provide several new examples of the $\{Mn(CO)_2\}^+$ fragment stabilized by $FPhNNS$ and $N_{Me}NS$; such dicarbonyls are usually stabilized only by phosphine ligands.
- f) A rational design of the ligand framework (R_1, R_2) may now lead to the desired NNS coordination motif in manganese carbonyls.

Acknowledgement

This research was supported by startup funds to MJR provided by the UT Austin College of Natural Sciences, the Welch Foundation (F-1822), the ACS Petroleum Research Fund (53542-DN13). SEL was the recipient of an Undergraduate Research Fellowship sponsored by the UT Austin Office of Research. The authors gratefully acknowledge Angela Spangenberg and Steve Sorey for technical assistance in acquiring VT NMR spectra. We also thank Dr Vince Lynch for assistance in the collection of X-ray data and refinement of structures.

Supporting Information

CIF files for all X-ray structures; VT ^1H NMR Spectrum of 1_{CO} (Fig. S1); disorder model for $5_{\text{CO-b}}$ (Fig. S2).

References

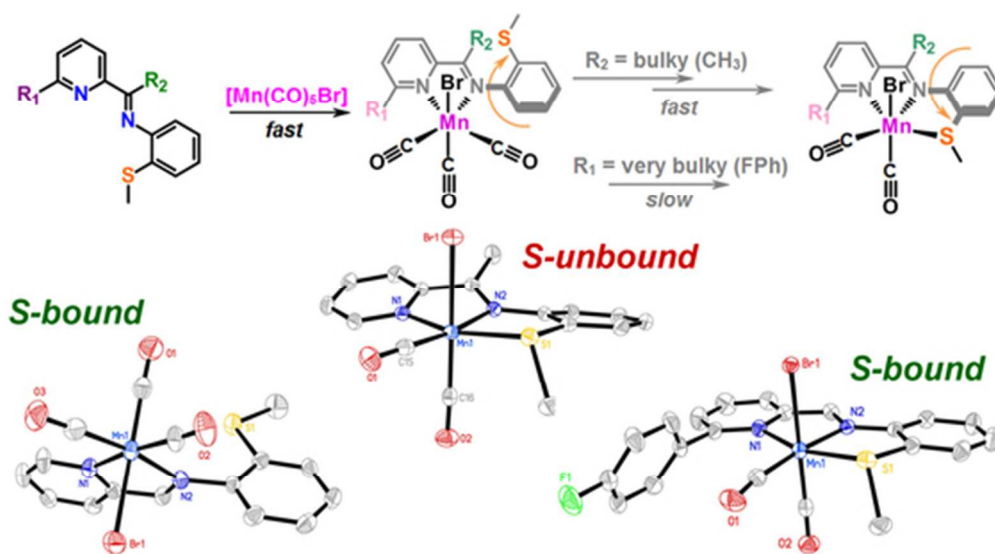
1. (a) C. Z. Li, E. Widjaja, and M. Garland, M. *Organometallics* 2004, **23**, 4131-4138. (b) R. D. Adams, K. Brosius and O. S. Kwon. *Inorg. Chem. Commun.* 2001, **4**, 671-673. (c) T. Kondo, Y. Sone, Y. Tsuji, and Y. J. Watanabe. *Organomet. Chem.* 1994, **473**, 163-173.
2. (a) S. Khabuanchalad, J. Wittayakun, R. J. Lobo-Lapidus, S. Stoll, R. D. Britt and B. C. Gates. *Langmuir*, 2013, **29**, 6279-6286. (b) R. Villaneau, A. Proust, F. Robert and P. Gouzerth. *Chem. Eur. J.* 2003, **9**, 1982-1990.
3. (a) G. Dordelmann, H. Pfeiffer, A. Birkner and U. Schatzschneider. *Inorg. Chem.* 2011, **50**, 4362-4367. (b) N. E. Brueckmann, M. Wahl, G. J. Reiss, M. Kohns, W. Watjen and P. C. Kunz. *Eur. J. Inorg. Chem.* 2011, 4571-4577. (c) G. Doerdelmann, T. Meinhardt, T. Sowik, A. Krueger and U. Schatzschneider. *Chem. Commun.* 2012, **48**, 11528-11530. (d) M. A. Gonzalez, N. L. Fry, R. Burt, R. Davda, A. Hobbs and P. K. Mascharak. *Inorg. Chem.* 2011, **50**, 3127-3134. (e) F. Mohr, J. Niesel, U. Schatzschneider and C. W. Lehmann. *Zeit. Anorg. Allg. Chem.* 2012, **638**, 543-546. (f) R. D. Rimmer, A. E. Pierri and P. C. Ford. *Coord. Chem. Rev.* 2012, **256**, 1509-1519. (g) A. E. Pierri, A. Pallaoro, G. Wu and P. C. Ford. *J. Am. Chem. Soc.* 2012, **134**, 18197-18200. (h) P. C. Ford. *Nitric Oxide Biol. Chem.* 2013, **34**, 56-64.
4. Y. Kuninobu and K. Takai. *Bull. Chem. Soc. Jap.* 2012, **85**, 656-671.
5. (a) S. K. Russell, A. C. Bowman, E. Lobkovsky, K. Wieghardt and P. J. Chirik. *Eur. J. Inorg. Chem.* 2012, *Special Issue*, 535-545. (b) F. Hartl, P. Rosa, L. Ricard, P. Le Floch and S. Zalis. *Coord. Chem. Rev.* 2007, **251**, 557-576. (c) F. Hartl and T. Mahabiersing. *Inorg. Chem.* 2003, **42**, 4442-4455. (d) W.-F. Liaw, C.-K. Hsieh, G.-Y. Lin and G.-H. Lee. *Inorg. Chem.* 2001, **40**, 3468-3475. (e) C.-M. Lee, G.-Y. Lin, C.-H. Hsieh, C.-H. Hu, G.-H. Lee, S.-M. Peng and W.-F. Liaw. *Dalton Trans.* 1999, 2393-2398. (f) W.-F. Liaw, C.-M. Lee, G.-H. Lee and S.-M. Peng. *Inorg. Chem.* 1998, **37**, 6396-6398. (g) F. Hartl. *Inorg. Chim. Acta* 1998, **268**, 1-11.
6. (a) Z. B. Mao, B. T. Gregg and A. R. Cutler. *Organometallics* 1998, **17**, 1993-2002. (b) Z. B. Mao, B. T. Gregg and A. R. Cutler. *J. Am. Chem. Soc.* 1995, **117**, 10139-10140. (c) M. B. Cavanaugh, B. T. Gregg and A. R. Cutler. *Organometallics* 1996, **15**, 2764-2769. (d) P. K. Hanna, B. T. Gregg and A. R. Cutler. *Organometallics* 1991, **10**, 31-33.
7. B. T. Gregg and A. R. Cutler. *Organometallics* 1994, **13**, 1039-1043.

8. (a) M. Bourrez, F. Molton, S. Chardon-Noblat and A. Deronzier. *Angew. Chem.* 2011, **50**, 9903-9906. (b) J. M. Smieja, M. D. Sampson, K. A. Grice, E. E. Benson, J. D. Froehlich and C. P. Kubiak. *Inorg. Chem.* 2013, **52**, 2484-2491.
9. (a) V. S. Thoi, Y. J. Sun, J. R. Long and C. J. Chang. *Chem. Soc. Rev.* 2013, **42**, 2388-2400. (b) J. G. McAlpin, T. A. Stich, W. H. Casey and R. D. Britt, R. D. *Coord. Chem. Rev.* 2012, **256**, 2445-2452. (c) S. Fukuzumi, D. C. Hong and Y. J. Yamada. *Phys. Chem. Lett.* 2013, **4**, 3458-3467. (d) R. Brimblecombe, A. Koo, G. C. Dismukes, G. F. Swiegers and L. Spiccia. *J. Am. Chem. Soc.* 2010, **132**, 2892. (e) D. J. Darensbourg and E. B. Frantz. *Inorg. Chem.* 2007, **46**, 5967-5978. (f) D. G. Nocera. *Acc. Chem. Res.* 2012, **45**, 767-776. (g) E. L. Warren, J. R. McKone, H. A. Atwater, H. B. Gray and N. S. Lewis. *Energy Environ. Sci.* 2012, **5**, 9653-9661.
10. D. Chen, R. Scopelliti and X. Hu, X. *Angew. Chem.* 2012, **51**, 1919-1921.
11. D. Chen, R. Scopelliti and X. Hu. *Angew. Chem.* 2011, **50**, 5671-5673.
12. T. B. Liu, B. Li, C. V. Popescu, A. Bilko, L. M. Perez, M. B. Hall and M. Y. Darensbourg. *Chem. Eur. J.* 2010, **16**, 3083-3089.
13. B. Li, T. Liu, C. V. Popescu, A. Bilko and M. Y. Darensbourg. *Inorg. Chem.* 2009, **48**, 11283.
14. P. J. Turrell, A. D. Hill, S. K. Ibrahim, J. A. Wright and C. J. Pickett. *Dalton Trans.* 2013, **42**, 8140-8146.
15. S. Kaur-Ghumaan, L. Schwartz, R. Lomoth, M. Stein and S. Ott. *Angew. Chem.* 2010, **49**, 8033-8036.
16. J. Connolly, A. R. J. Genge, S. D. Orchard, S. J. A. Pope and G. Reid, G. *J. Chem. Soc. Dalton Trans.* 1999, 2343-2351.
17. H. Elias, G. Schmidt, H.-J. Küppers, M. Saher, K. Wieghardt, B. Nuber and J. Weiss. *Inorg. Chem.* 1989, **28**, 3021-3024.
18. J. Connolly, G. W. Goodban, G. Reid and A. M. Z. Slawin. *J. Chem. Soc. Dalton Trans.* 1998, 2225-2231.
19. S.-T. Liu, H.-E. Wang, L.-M. Yin, S.-C. Tsai, K.-J. Liu, Y.-M. Wang, M.-C. Cheng and S.-M. Peng. *Organometallics* 1993, **12**, 2277-2283.
20. W. Levason, L. P. Ollivere, G. Reid, N. Tsoureas and M. Webster. *J. Organomet. Chem.* 2009, **694**, 2299-2308.

21. B. Patel and G. Reid. *Dalton Trans.* 2000, 1303-1307.
22. Compain, J.-D.; Bourrez, M.; Haukka, M.; Deronzier, A.; Chardon-Noblat, S. *Chem. Commun.* **2014**, 50, 2539-2542.
23. M. A. Gonzalez, S. J. Carrington, N. L. Fry, J. L. Martinez and P. K. Mascharak. *Inorg. Chem.* 2012, **51**, 11930-11940.
24. S. J. Carrington, I. Chakraborty and P. K. Mascharak, P. K.. *Chem. Commun.* 2013, *ASAP*.
25. M. A. Gonzalez, M. A. Yim, S. Cheng, A. Moyes, A. J. Hobbs and P. K. Mascharak. *Inorg. Chem.* 2012, **51**, 601-608.
26. B. W. Skelton, V.-A. Tolhurst, A. H. White, A. M. Williams and A. J. Wilson. *J. Organomet. Chem.* 2003, **674**, 38-44.
27. S. K. Chatterjee, S. Roy, S. K. Barman, R. C. Maji, M. M. Olmstead and A. K. Patra. *Inorg. Chem.* 2012, **51**, 7625-7635.
28. S. Roy, P. Mitra and A. K. Patra. *Inorg. Chim. Acta* 2011, **370**, 247-253.
29. F. H. Kohler, N. Hebenanz, G. Muller, U. Thewalt, B. Kanellakopulos and R. Klenze. *Organometallics* 1987, **6**, 115.
30. S. Pohl, W. Saak and P. Z. Stolz. *Naturforsch. B Chem. Sci.* 1988, **43**, 171.
31. A. N. Chekov. *Zh. Neorg. Khim.* 2006, **51**, 2026.
32. O. Seewald, U. Florke, G. Henkel and T. Seshadri. *Acta Crystallogr. E* 2005, **61**, m1948.
33. K. Ha. *Z. Kristallogr. New Cryst. Struct.* 2011, **226**, 518.
34. K. D. Welch, W. G. Dougherty, W. S. Kassel, D. L. DuBois and R. M. Bullock. *Organometallics* 2010, **29**, 4532-4540.
35. W. A. King, B. L. Scott, J. Eckert and G. J. Kubas. *Inorg. Chem.* 1999, **38**, 1069-1084.
36. W. A. King, X.-L. Luo, B. L. Scott, G. J. Kubas and K. W. Zilm. *J. Am. Chem. Soc.* 1996, **118**, 6782-6783.

Table 1. Crystal data and refinement parameters.

	2_{CO} [(OMeNNS)Mn(CO) ₃ Br]	3_{CO}•CH₂Cl₂ [(MeNNS)Mn(CO) ₃ Br] •CH ₂ Cl ₂	3_{Br} [(MeNNS)Mn(Br) ₂]	4_{CO} [(N _{Me} NS)Mn(CO) ₂ Br]	5_{CO-a} [(FPhNNS)Mn(CO) ₃ Br]	5_{CO-b} [(FPhNNS)Mn(CO) ₂ Br]
formula	C ₁₇ H ₁₄ N ₂ O ₄ BrSMn	C ₁₈ H ₁₆ N ₂ O ₃ BrSMn	C ₁₄ H ₁₄ N ₂ Br ₂ SMn	C ₁₆ H ₁₄ BrMnN ₂ O ₂ S	C ₂₂ H ₁₅ N ₂ O ₃ SBrFMn	C ₂₁ H ₁₅ N ₂ O ₂ SBrFMn
FW	477.21	546.14	457.09	433.20	541.27	512.14
color	red	red	orange	black	orange	black
habit	plate	block	block	needle	plate	needles
size (mm)	0.36 × 0.21 × 0.09	0.65 × 0.41 × 0.11	0.30 × 0.14 × 0.09	0.27 × 0.21 × 0.12	0.34 × 0.23 × 0.11	0.17 × 0.13 × 0.08
<i>T</i> (K)	163(2)	163(2)	173(2)	153(2)	153(2)	100(2)
λ (Å)	0.71073	0.71073	0.71073	0.71073	0.71073	0.71073
lattice	triclinic	triclinic	monoclinic	monoclinic	monoclinic	monoclinic
space group	<i>P</i> $\bar{1}$	<i>P</i> $\bar{1}$	<i>P</i> ₂ 1/n	<i>P</i> ₂ 1/n	<i>P</i> ₂ 1/n	<i>P</i> ₂ 1/c
<i>a</i> (Å)	7.5300(3)	8.7613(3)	11.838(3)	8.7752(19)	7.9074(5)	13.942(5)
<i>b</i> (Å)	7.6723(3)	10.8921(4)	10.124(3)	12.659(3)	21.6449(14)	11.412(5)
<i>c</i> (Å)	17.7327(6)	13.0888(5)	13.654(4)	14.644(3)	12.5018(6) Å	14.573(4)
α (deg)	87.250(2)	66.319(2)	90	90	90	90
β (deg)	79.371(2)	79.790(2)	102.610(7)	92.798(5)	96.094(2)	117.66(3)
γ (deg)	66.350(2)	69.483(2)	90	90	90	90
<i>V</i> (Å ³)	921.93(6)	1070.35(7)	1596.9(8)	1624.8(6)	2127.7(2)	2053.7(13)
<i>Z</i>	2	2	4	4	4	4
<i>d</i> _{calc} (g/cm ³)	1.719	1.695	1.901	1.771	1.690	1.656
μ (mm ⁻¹)	3.021	2.852	5.952	3.409	2.632	2.718
GOF on <i>F</i> ²	1.122	1.031	0.999	1.112	1.121	1.110
<i>R</i> indices	<i>RI</i> = 0.0232	<i>RI</i> = 0.0350	<i>RI</i> = 0.0872	<i>RI</i> = 0.0310	<i>RI</i> = 0.0284	<i>RI</i> = 0.0553
[<i>I</i> > 2 σ (<i>I</i>)]	<i>wR2</i> = 0.0676	<i>wR2</i> = 0.0792	<i>wR2</i> = 0.2012	<i>wR2</i> = 0.0735	<i>wR2</i> = 0.0661	<i>wR2</i> = 0.1205
<i>R</i> indices	<i>RI</i> = 0.0273	<i>RI</i> = 0.0412	<i>RI</i> = 0.1217	<i>RI</i> = 0.0365	<i>RI</i> = 0.0411	<i>RI</i> = 0.0725
all data	<i>wR2</i> = 0.0700	<i>wR2</i> = 0.0842	<i>wR2</i> = 0.2242	<i>wR2</i> = 0.0759	<i>wR2</i> = 0.0710	<i>wR2</i> = 0.1280



Manganese carbonyls are ligated by Pyridine/Thioether Schiff base (NNS) ligands. Coordination of the thioether-S donor to the Mn(I) center is determined by subtle steric changes at the ligand periphery.
47x26mm (300 x 300 DPI)